REPORT DOCUMENTATION PAGE

Form Approved
OMB No. 0704-0188

1. REPORT DATE *(DD-MM-YYYY)*	**2. REPORT TYPE**	**3. DATES COVERED** *(From - To)*
05/29/2015	Final Technical Report	06/01/2012 - 05/31/2015

4. TITLE AND SUBTITLE

Dielectric Metamaterials

5a. CONTRACT NUMBER

5b. GRANT NUMBER

N00014-12-1-0722

5c. PROGRAM ELEMENT NUMBER

6. AUTHOR(S)

Krishnamurthy, Srini
Slovick, Brian
Yu, Zhi Gang

5d. PROJECT NUMBER

P21340

5e. TASK NUMBER

5f. WORK UNIT NUMBER

7. PERFORMING ORGANIZATION NAME(S) AND ADDRESS(ES)

SRI International
333 Ravenswood Avenue
Menlo Park, CA 94025

8. PERFORMING ORGANIZATION REPORT NUMBER

9. SPONSORING / MONITORING AGENCY NAME(S) AND ADDRESS(ES)

Office of Naval Research
Code 33
875 N. Randolph Street
Arlington, VA 22203-1995

10. SPONSOR/MONITOR'S ACRONYM(S)

ONR

11. SPONSOR/MONITOR'S REPORT NUMBER(S)

12. DISTRIBUTION / AVAILABILITY STATEMENT

Distribution A; Approved for Public Release; distribution unlimited

13. SUPPLEMENTARY NOTES

14. ABSTRACT

In this program we (a) developed an analytical theory—generalized effective medium— for accurately calculating the effective permittivity and permeability of dielectric metamaterials (MMs) near the Mie resonances ; (b) modeled and designed submicron-thick perfect MM reflectors based on silicon Mie resonators ; (c) demonstrated near-perfect reflection in collaboration with Vanderbilt University; and (d) developed an semi-analytical theory (called g-delta method) of both random and controlled disorder in MMs that predicts anisotropic and inter-polarization scattering by submicron-thick MM layers containing all-isotropic constitutive materials.

15. SUBJECT TERMS

metamaterials, dielectric, Mie resonances, single negative metamaterial, perfect reflection, perfect polarizer,

16. SECURITY CLASSIFICATION OF:			**17. LIMITATION OF ABSTRACT**	**18. NUMBER OF PAGES**	**19a. NAME OF RESPONSIBLE PERSON**
a. REPORT	**b. ABSTRACT**	**c. THIS PAGE**			Srini Krishnamurthy
U	U	U	SAR	30	**19b. TELEPHONE NUMBER** *(include area code)* 650-859-4997

Final Report • 29 May 2015

Dielectric Metamaterials

SRI Project P21340

ONR Contract N00014-12-1-0722

Prepared by:

Srini Krishnamurthy, Senior Principal Scientist
Applied Physical Sciences Laboratory

Prepared for:

Office of Naval Research
Code 33
875 N. Randolph Street
Arlington VA 22203-1995

Attention: Dr. Mark Spector

CONTENTS

EXECUTIVE SUMMARY

The objectives of this ONR-funded project, as stated in our original proposal, are to: (1) acquire a fundamental understanding of the scattering from isolated resonant elements and establish design rules for desired properties; (2) explore ways to reduce the size of the resonating elements from that required for Mie scattering and achieve this without requiring higher-index material or higher-index contrast than currently available; (3) vary electrical and magnetic resonance independently to achieve refractive index of our choice, (4) develop a theory that will accurately assess the impact of various forms of disorder on metamaterials (MMs) (both dielectric and metal inclusions); and (5) identify designs that exploit the novel MM properties developed in the program and experimentally confirm the performance of one or more novel structures. The SRI team—Brian Slovick, Zhi Gang Yu (currently at Washington State University, Pullman, WA) and Srini Krishnamurthy—has completed all these tasks, published some of the results,[1-4] and is currently preparing the remaining results for publication.[5-7]

Accomplishments of the program include: (a) development of an analytical theory—generalized effective medium or GEM theory— for accurately calculating the effective permittivity and permeability of dielectric MMs near the Mie resonances[1]; (b) modeling and design of submicron-thick perfect MM reflectors based on silicon Mie resonators[2]; (c) demonstration of near-perfect reflection in collaboration with Vanderbilt University[3,4]; and (d) development of an analytical theory of both random and controlled disorder in MMs that predicts *anisotropic* and *interpolarization* scattering by submicron-thick MM layers containing *all-isotropic* constitutive materials[5,6]. A dielectric MM polarizer based on these results is currently being verified at Vanderbilt University.[7]

This study resulted in the development of disorder theory of metamaterials for both specular reflection and diffuse scattering:

1. We developed an analytical method (the Generalized Effective Medium [GEM] model) and a generalized semi-analytical model (the g-δ method) to include disordered spheres in simple cubic arrangement in a medium, and carried out several numerical studies with an accurate numerical code (HFSS) from ANSYS, Inc. In contrast with previous models[8,9,] the GEM model includes the interaction of the single-particle Mie resonance with the background and shows noticeable improvement over those models[8,9] for various dielectric contrasts and volume-loading densities. The GEM model also predicts the anti-resonance effect in agreement with HFSS. The generalized g-δ method for spheres includes size disorder and lattice disorder. We have integrated this method with HFSS to include large disorder.
2. We studied the effect of disorder on diffuse scattering, in addition to the specular reflection described earlier. Specific achievements include (a) distinguishing effective medium and diffusive scattering regimes and providing quantitative criteria to identify each regime; (b) development of suitable theories for these regimes; (c) discovery of a new phenomenon; i.e., that the location disorder can cause local anisotropy, which in turn profoundly effects light propagation in the effective-medium regime; (d) development of an analytical theory of vacancy scattering based on our previously published effective-

medium theory, and (e) development of an analytical solution based on diffusion equations, applicable in the diffusive scattering regime.

Finally, we applied our theory and identified two new concepts that exploit Mie scattering in dielectric shapes.

1. We developed designs for single-layer all-dielectric MM slabs that produce near-perfect reflection with virtually no absorption.[1] The Vanderbilt team fabricated the structures and demonstrated near-perfect reflection with a single layer of Si cylinders on SOI substrate.[3] It is important to note that perfect *reflection* is obtained using Si and SiO_2, which are fully *transparent* in this wavelength regime.
2. Our GEM model and an all-analytical approach[5,6] helped us gain physical understanding of *anisotropic* optical property of the disordered MM made of *all-isotropic* constituents. With additional use of accurate finite-element electromagnetic (EM) simulations, SRI has identified a single-layer design of dielectric and isotropic Mie scatterers to effectively reflect one polarization while transmitting the other. In other words, this single layer made of isotropic material behaves likes an anisotropic material and efficiently performs the function of polarizer. The design is not yet optimized, and this principle can be applied also to develop designs for polarization rotation in which the scattering between *s* and *p* polarization is preferentially and controllably enhanced as needed. A dielectric MM polarizer design has been provided to Vanderbilt University for fabrication and testing. Once we have verified the results, we will summarize them for publication.[7]

TECHNICAL DISCUSSION

1. Background

The ability to derive a composite medium with optical properties much different from those of the constitutive materials makes MMs of considerable scientific and technological interest. Over the last decade, as the operating frequency of MMs has progressed from GHz and THz to infrared and visible, these materials have exploited the magnetic-dipole resonance in the split-ring resonator to achieve negative permeability and the electric-dipole resonance in metallic wires to achieve negative permittivity. The extension of these traditional MM design principles to infrared and visible frequencies has been limited primarily by the absorption loss and fabrication complexity associated with the metallic elements. All-dielectric MMs offer the possibility of achieving properties similar to those of their metallic counterparts but with substantially less absorption loss and fabrication complexity. O'Brien and Pendry[10] were the first to exploit Mie resonance to obtain a bulk magnetic polarization in an array of dielectric cylinders.

2. Theory of Metamaterials

In a truly homogeneous medium, the values of permittivity (ε) and permeability (μ) do not depend on the ordering of the constituents. In interacting systems with Mie scatterers in close proximity, the disorder will play a major role in determining the material properties. Hence, it is necessary to develop a theory and approach to systematically evaluate the effect of disorder on permittivity, permeability, and optical properties of MMs. We have developed models to gain an understanding of disorders in MMs in four sequential steps—all-analytical, semi-analytical,

hybrid method, and measurement. We used the measurement step to validate the accuracy of our calculational methods.

2.1 Analytical Model

2.1.1 Effective Medium

Metamaterials possessing unusual values of permittivity and magnetic permeability exhibit unique responses to electromagnetic waves and promise many novel applications. Reliable and efficient modeling tools play an indispensable role in advancing the field of MMs. The existing models generally fall into two categories: the finite-element (e.g., HFSS) and the finite-difference time-domain (FDTD). While nearly exact, these codes are time-consuming to use and often ambiguous in extracting the effective permittivity and permeability of a composite. The other approach is to develop an analytical effective medium (EM) model.[8] While these models are simple, intuitive, and fast, they have limited range validity due to the approximations invoked to obtain an analytic solution. In addition, because a composite, by definition, has a spatial inhomogeneity with a length scale of *a* (where *a* is the distance between inclusions), a spatial dispersion arises that produces the frequently observed anti-resonance, in which a resonance in ε (μ) is accompanied by an "inverted" resonance in μ (ε) at the same frequency. These anti-resonances are absent in conventional effective medium theories in which the frequency, ω-dependent $\varepsilon(\omega)$ and μ (ω), are decoupled. Moreover, when the composite is considered an effective media, the wavelengths λ and λ_0 in the media and in vacuum are related via the effective refractive index, $\lambda=\lambda_0/n_{\text{eff}}$. In the most popular EM model developed by Lewin,[8] n_{eff} can become arbitrarily large at the resonance in ε or μ, which leads to $\lambda/a << 1$, in contradiction with the approximation of the model ($\lambda/a >> 1$).

Because of the limitations of EM models, considerable efforts have been devoted to improving them. One such effort is given in which a zero-scattering condition is imposed on a core-shell structure[8] (referred here as Wu model), with the core representing the inclusion and the shell representing the host, to find the effective ε and μ. While these models are certainly an improvement over the Lewin model, the long-wavelength approximation used here introduces several issues in the application; specifically, the physics of spatial dispersion is not adequately captured, the anti-resonance is absent, and n_{eff} can be divergent.

We derived a GEM model by considering the same core-shell structure without invoking the long-wavelength approximation. By changing variables, we were able to obtain separate equations for *n* and *z*, thus allowing an unambiguous determination of the effective ε and μ. The GEM model is shown to be valid over a much broader range and adequately captures the spatial dispersion effect. The reason that the GEM model is more accurate than the Lewin and other models is that it includes non-uniform

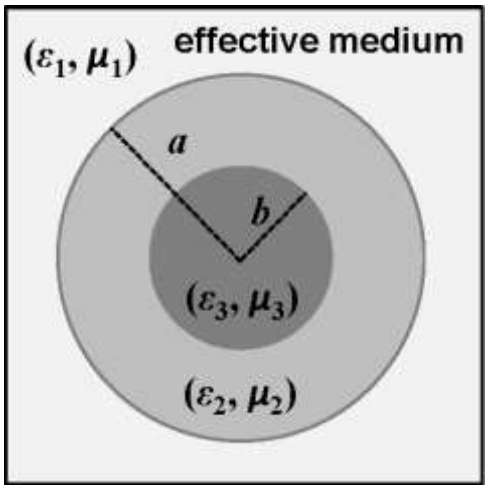

Figure 1. Definition of terms for the GEM model.

electromagnetic fields and resonances in the surrounding shell medium.

In the GEM model approach, dielectric spheres with ε_3 and μ_3 are dispersed in a medium with ε_2 and μ_2. If the core-shell structure is embedded in the true effective medium with ε_1 and μ_1, then the core-shell as shown in Figure 1 should not cause any scattering of electromagnetic waves. In other words, our goal is to find the effective ε_1 and μ_1 outside the core-shell so that no scattering takes place; i.e., the forward-scattering amplitude $S(0)$ is zero:

$$S(0) = a_1(0) + b_1(0) = 0, \tag{1}$$

where a_1 and b_1 are the electric- and magnetic-dipolar Lorentz-Mie scattering coefficients of the core-shell structure. Using the well-known[11] form of a_1 and b_1 for the core-shell structure, we set each of them equal to zero (to achieve S(0)=0), and after extensive algebraic manipulations, we arrived at two conditions:

$$\frac{\psi_1(k_1a)}{\psi_1'(k_1a)} = \frac{G_\varepsilon(k_2a)G_\mu(k_2a)}{G_\varepsilon'(k_2a)G_\mu'(k_2a)}, \tag{2}$$

$$z_1 = z_2\left[\frac{G_\varepsilon'(k_2a)G_\mu(k_2a)}{G_\varepsilon(k_2a)G_\mu'(k_2a)}\right]^{1/2}, \tag{3}$$

where $k_i=\omega/c(\varepsilon_i\mu_i)^{1/2}$(i=1,2,3) and

$$\begin{aligned}
&\psi_1(x) = xj_1(x)\\
&\chi_1(x) = -xy_1(x)\\
&G_{\varepsilon(x)} = \psi_1(x) - A_1\chi_1(x)\\
&G_{\mu(x)} = \psi_1(x) - B_1\chi_1(x)
\end{aligned} \tag{4}$$

with spherical Bessel functions j_1, y_1, A_1, and B_1 having the same form described in the literature.[11] Note that by including only a_1 and b_1, we are implicitly assuming the dipole approximation (that is a_n and b_n are zero for $n > 1$).

In the limit at which the wavelength in the effective medium is much larger than the unit cell diameter (i.e., $k_1a<<1$), the Riccati-Bessel functions can be replaced by their small-argument approximations,[11] and Eq. (2) reduces to

$$\frac{1}{2}k_1a = \frac{G_\varepsilon(k_2a)G_\mu(k_2a)}{G_\varepsilon'(k_2a)G_\mu'(k_2a)}. \tag{5}$$

From Eqs. (3) and (5), and noting that $k_1=n_1k_0$, where $k_0=\omega/c$, then ε_1 and μ_1 of the metamaterial can be calculated from the auxiliary equations

$$\mu_1 = n_1z_1 \text{ and } \varepsilon_1 = n_1/z_1 . \tag{6}.$$

After straightforward algebraic manipulations, it can be shown that these expressions reduce to those derived by Wu et al.[8]

If we make the additional approximation that the wavelength in the shell region is also large compared to the unit cell diameter (i.e., $k_2a<<1$ and thus $k_2b<<1$), while k_3b remains arbitrary, the functions $G_\varepsilon(x)$ and $G_\mu(x)$ on the right-hand side of Eqs. (2) and (3) can also be expanded in x. The resulting equations can be solved to obtain closed-form solutions for μ_1 and ε_1 that are equivalent to the popular Lewin effective-medium model.[8]

To illustrate the improved accuracy of our GEM model compared to Lewin or Wu models, we plot in Figure 2 the calculated effective permittivity and permeability for two cases—high and low permittivity contrast—as a function of a/λ, where a is the unit cell length of the cubic lattice and λ is the wavelength.

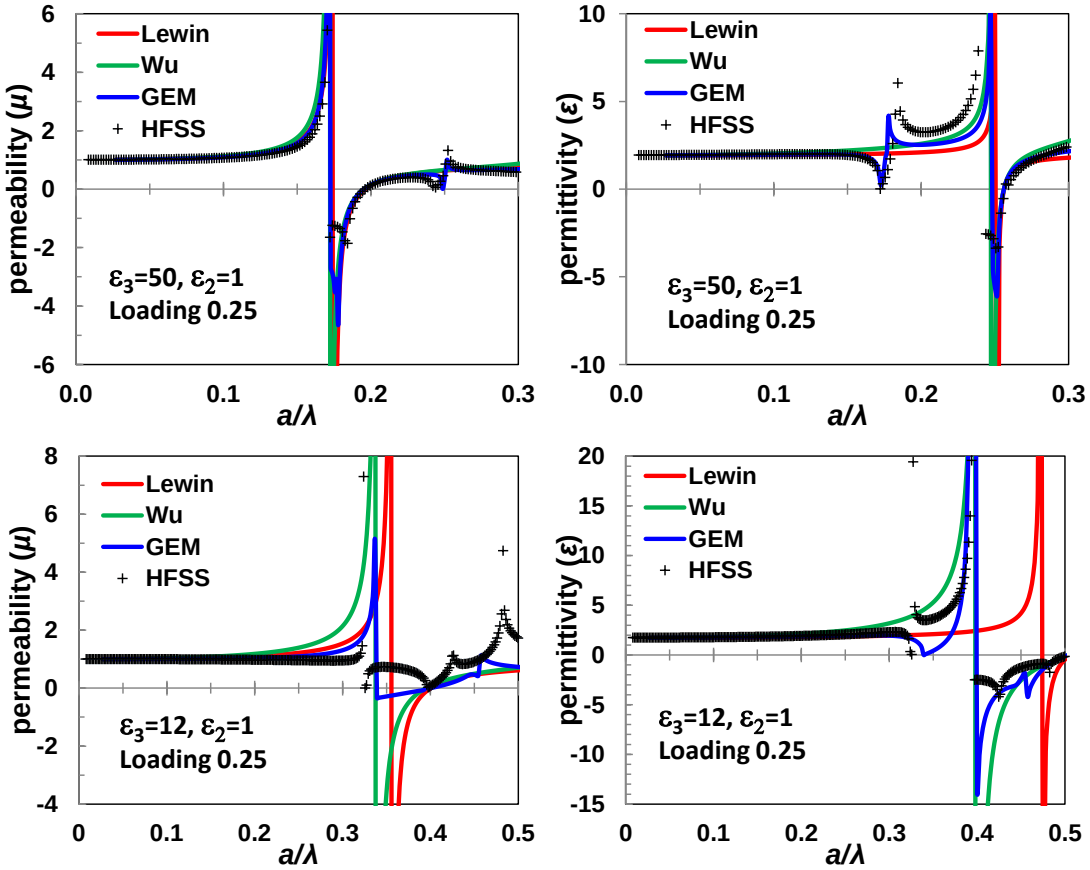

Figure 2. Comparison of calculated Re(μ) and Re(ε) versus a/λ for the GEM (blue), Wu (green), Lewin (red) models to HFSS (symbol) calculations. Top panel (ε_3=50, ε_2=1) and bottom panel (ε_3=12, ε_2=1).

In the high-contrast case (with ε_3=50 and ε_2=1, top panel), in which the long-wavelength approximation is valid, all three models appear to give nearly identical results when compared to the finite-element calculations from HFSS results. However, a careful comparison indicates that the other models do not reproduce the anti-resonance in permittivity (seen near a/λ=0.1) and in permeability (near a/λ near 0.15). Only GEM agrees with the HFSS results. In the low-contrast case (with ε_3=12 and ε_2=1, corresponding to Si in the short-wave infrared or SWIR, bottom panel), in which the long-wavelength approximation is not valid, the results from Wu and Lewin models differ considerably from the HFSS values. The values obtained by GEM are much closer to the HFSS values and predict 1st resonance ε and μ and the anti-resonance in permittivity (a/λ

near 0.3). In both cases, the Wu and GEM models predict resonant frequencies correctly and in agreement with HFSS. However, the value at the resonance is infinite in the Lewin and Wu models and finite in GEM model, which is in better agreement with HFSS. Overall the analytical expression provided by our GEM model is in very good agreement with the more-accurate but time-consuming HFSS calculations.

In summary, our model is a self-consistent GEM model for metamaterials containing spherical particles. It adequately captures the physics of spatial dispersion and predicts anti-resonance and finite n_{eff}. The model provides significant improvement over conventional effective-medium theories and, more importantly, captures the effects of spatial-dispersion while retaining the mathematical clarity. It predicts a finite effective refractive index and anti-resonance in permittivity and permeability. Its superior accuracy enables a reliable tool to model and design metamaterials. These results were published[2] in *Physical Review*. The extension of the model to shapes other than spheres may not be possible.

2.1.2 Vacancies in Effective Medium

In the GEM model, the effective parameters are derived from the condition that the spherical unit cell of the composite, shown in Figure 3, is equivalent to a homogeneous sphere of unknown ε_{eff} and μ_{eff}.

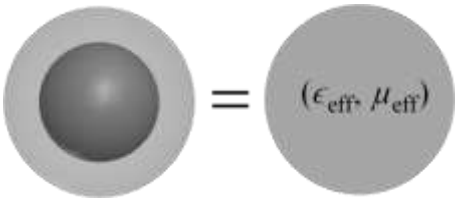

Figure 3. Effective homogeneous medium for a composite of spherical particles.

This statement is equivalent to the condition that the unit cell of the composite, embedded in the effective medium, should have a scattering cross section of zero.[12] The latter condition reduces to two coupled nonlinear equations in the variables ε_{eff} and μ_{eff}. To decouple these equations, various long-wavelength approximations have been employed. In our approach, the equations are decoupled by changing variables to the index $n_{eff}=\sqrt{(\varepsilon_{eff}\mu_{eff})}$ and impedance $z_{eff}=\sqrt{(\mu_{eff}/\varepsilon_{eff})}$. This leads to a closed-form expression for z_{eff} and a nonlinear equation for n_{eff}, which can be readily solved in MATLAB. By comparison to full-wave calculations in HFSS, it has been shown that the GEM model is more accurate close to the Mie resonances and at higher frequencies compared to existing theories. Figure 4 shows the hierarchy of the effective-medium theories and their levels of approximation.

All theories follow from the condition that the scattering cross section of the unit cell in the effective medium is zero. The approximation used in the GEM model is to include only the first two terms (electric and magnetic dipole) in the expression for the scattering cross section. In the model developed by Wu et al.,[9] it is assumed that the wavelength in the effective medium is much larger than the unit cell. The popular model developed by Lewin[8] assumes that the wavelength in the background (shell) region is also large compared to the unit cell diameter, and the Maxwell-Garnett model is obtained by assuming that the wavelength in the sphere (core) region is also large relative to the unit cell.

The effective-medium theories described above, including our GEM model, are derived from the zero-scattering condition. Since such a condition is satisfied only for a perfect periodic lattice, the effective-medium theories implicitly assume periodicity. On the other hand, it may be useful to quantify the impact of deviations from the perfect lattice on the zero-scattering condition.

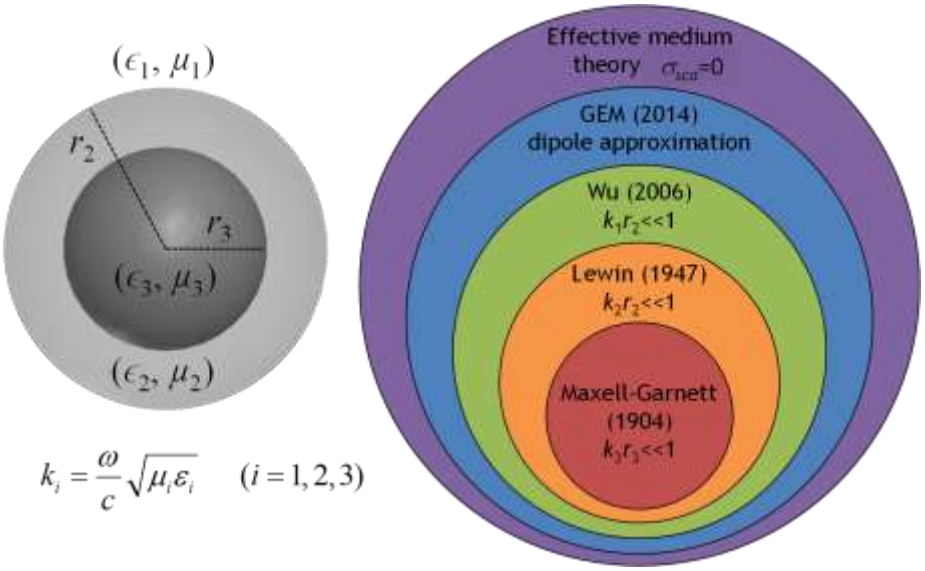

Figure 4. Hierarchy of the effective-medium theories along with their approximations.

One possible source of scattering is vacancies, or absences of a sphere in the lattice. Figure 5 illustrates how vacancies may be modeled as a perturbation of the effective-medium theory. Figure 5(a) shows the perfect periodic lattice and its equivalent homogenous effective medium, which may be calculated accurately using the GEM model. Figure 5(b) shows the same lattice, but with one sphere missing (i.e., a vacancy). To determine the scattering due to the vacancy, the scattering cross section is calculated for a single sphere of permittivity ε_1, embedded in the effective medium (a similar argument applies to the permeability). The physical consequences of this method are immediately clear: Vacancy scattering worsens when the effective permittivity differs significantly from the background permittivity ε_1. This may occur, for example, at high loading densities or for spheres with large permittivity, or near the Mie resonances, where the effective permittivity exhibits Lorentzian-like resonances.

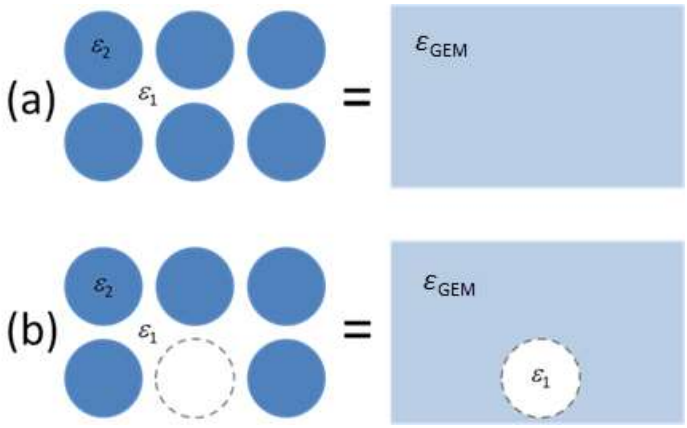

Figure 5. Illustration of a perfect periodic effective medium (a) and the effective medium with a defect void (b).

When the density of vacancies is small, the effective permittivity of the background medium is approximately unchanged, and the scattering from the vacancies can be approximated by the equations for single-particle Mie scattering.[13] In this case, the scattering cross section is calculated for the case shown in Figure 5(b). The mean free path Λ is related to the vacancy density N and cross section as

$$\Lambda = (\sigma N)^{-1} \tag{8}$$

For example, consider spheres of radius 0.12 μm, with ε_2=50 embedded in vacuum (ε_1=1) with a loading density of 25%. The effective permittivity and permeability from the GEM model are shown in Figures 6a and 6b, respectively. Figure 6c shows the mean free path, normalized to the unit cell length *a*, for a vacancy density of 1 %. Away from the Mie resonances, where the effective permittivity is similar to the void permittivity, the scattering is weak and the mean-free path is much greater than the unit cell length. In these regions, the composite behaves as a specular homogenous medium even for thick samples. On the other hand, near the Mie resonances, the permittivity and permeability of the background differ significantly from those of the void, leading to more scattering and a reduced mean-free path. In these regions, the mean-free path is of the order of the unit cell length, indicating that the composite will behave diffusively even if the material is just a few unit cells thick.

The conclusions are similar for spheres with lower permittivity. Figure 7 shows the permittivity (a) and permeability (b), calculated from the GEM model, for spheres of radius 0.2 μm, with ε_2=12 embedded in vacuum (ε_1=1) for a loading density of 25%. The mean-free path for a

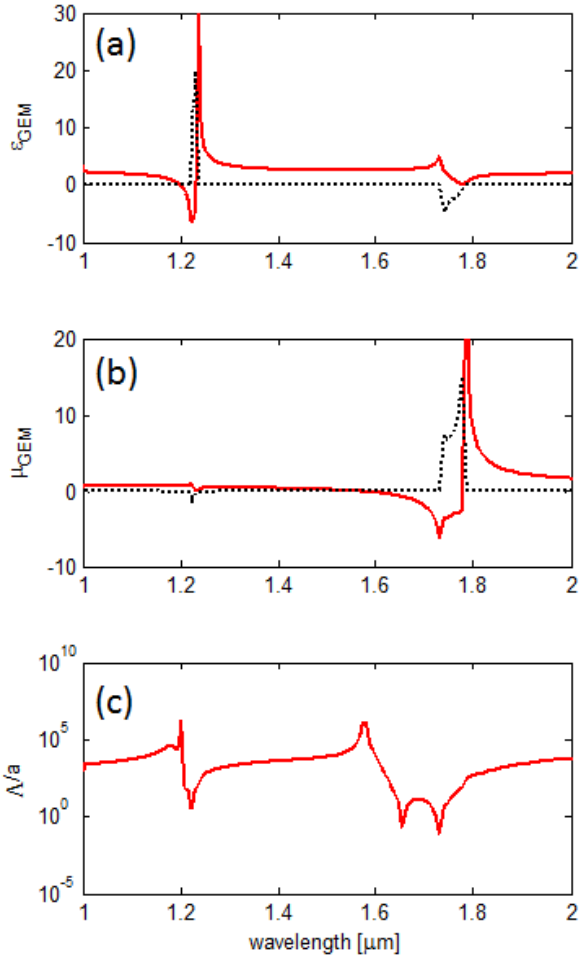

Figure 6. Effective ε (a) and μ (b) from GEM model for spheres of radius 0.12 μm, with ε_2=50 in vacuum (ε_1=1) with a loading density of 25%, and the mean-free path (normalized to a) for 1% vacancy density (c).

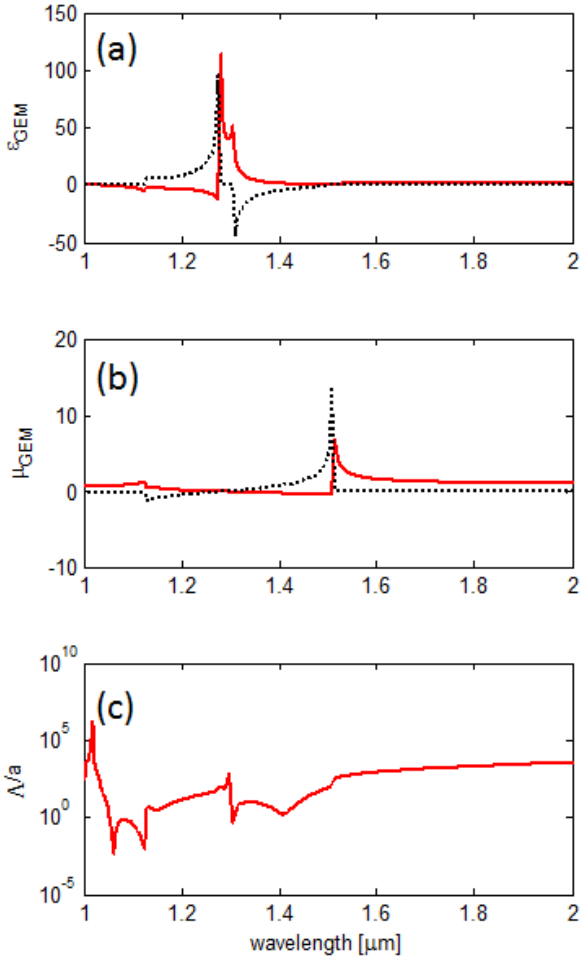

Figure 7. Effective ε (a) and μ (b) from GEM model for spheres of radius 0.2 μm, with ε_2=12 in vacuum (ε_1=1) with a loading density of 25%, and the mean-free path (normalized to a) for 1% vacancy density (c).

vacancy density of 1% is shown in Figure 7c. Similar to spheres with larger permittivity, the scattering due to vacancies is negligible, except very close to the Mie resonances. Additional calculations have shown that the scattering reduces (or the mean-free path increases) as the loading density of spheres decreases, since in this case the effective parameters are closer to those of the void.

2.1.3 Analytical Model Diffuse Medium

The tacit assumption in our approach is that the system can be adequately described by a homogeneous material with spatially independent effective values for ε and μ (i.e., the effective-medium regime). Within the effective-medium approximation, light reflection and transmission at the interface follow a well-defined direction (specular), and light scattering into other directions is neglected.

When disorder or imperfection in a material composite is included, a conceptual difficulty arises. On the one hand, the disorder will cause strong light scattering (e.g., rough surface in a bulk material), and on the other hand, the effective-medium approximation used for metamaterial research would exclude all scattering. This intrinsic inconsistency indicates that, to adequately account for the disorder effect, one may have to go beyond the effective-medium approximation. While it is true that scattering is present in an ordered composite, the constructive interference among different light rays accentuates the specular direction, making scattering into other directions negligible. In a disordered system, the constructive interference is much weakened, and the scattering issue becomes acute. When the scattering is sufficiently strong, the system becomes turbid and light propagation is diffusive. Researchers often resort to solving the radiative transfer equation or using numerical Monte-Carlo codes such as *LightTools.* Below we develop an analytical approach to calculate the diffused scattering and show that it agrees with the results obtained with *LightTools*.

The diffusion equation for a photon fluence rate Φ [W/cm^2] is given by[14]

$$\frac{1}{c}\frac{\partial\Phi(\vec{r},t)}{\partial t}+\mu_a\Phi(\vec{r},t)-\nabla\cdot\left[D\nabla\Phi(\vec{r},t)\right]=S(\vec{r},t)\,, \tag{9}$$

where S is the light source, μ_a is the absorption coefficient [cm^{-1}], and D is the diffusion constant [cm]

$$D=\left[3(\mu_a+\mu'_s)\right]^{-1}=\frac{1}{3}\Lambda\,, \tag{10}$$

where Λ [cm^{-1}] is the mean-free path [cm] and

$$\mu'_s=(1-g)\mu_s \tag{11}$$

is the reduced scattering coefficient, where g is the scattering anisotropy parameter. In the diffusion approximation, the radiance [W/cm^2/Sr] is given by

$$L(\vec{r},\hat{s},t)=\frac{1}{4\pi}\Phi(\vec{r},t)-\frac{3}{4\pi}D\nabla\Phi(\vec{r},t)\cdot\hat{s} \tag{12}$$

where *s* is a unit vector in the direction of scattering. The first term represents the isotropic "Lambertian" contribution and the second term is an anisotropic correction. Assuming steady state, one dimension, and no sources, the diffusion equation reduces to

$$\mu_a \Phi(x) - D\frac{d^2\Phi(x)}{dx^2} = 0. \tag{13}$$

The solution to Eq. (13) is

$$\Phi(x) = C_1 \exp(\alpha x) + C_2 \exp(-\alpha x) \tag{14}$$

where C_1 and C_2 are constants determined by the boundary conditions and

$$\alpha \equiv (\mu_a / D)^{1/2}. \tag{15}$$

For the boundary conditions[15]

$$\Phi(0) = \Phi_0 \quad \text{and} \quad \Phi(d) = 0, \tag{16}$$

the photon fluence rate can be written as

$$\Phi(x) = \Phi_0 \frac{\sinh\left[\alpha(d-x)\right]}{\sinh(\alpha d)}. \tag{17}$$

From Eq. (4), the radiance is then given by

$$L(x,\beta) = \frac{1}{4\pi}\Phi(x) - \frac{3D}{4\pi}\frac{d\Phi(x)}{dx}\beta = \frac{\Phi_0}{4\pi}\frac{\sinh\left[\alpha(d-x)\right]}{\sinh(\alpha d)} + 3\alpha D\frac{\Phi_0}{4\pi}\frac{\cosh\left[\alpha(d-x)\right]}{\sinh(\alpha d)}\beta, \tag{18}$$

where β=cosθ is the direction cosine for the scattered light. The forward- and backward-diffusing intensities are given by

$$I^{\pm 1}(x) = \int_0^{\pm 1} d\beta L(x,\beta)\beta = \frac{\Phi_0}{4}\frac{\sinh[\alpha(d-x)]}{\sinh(\alpha d)} \pm \frac{\alpha D\Phi_0}{2}\frac{\cosh[\alpha(d-x)]}{\sinh(\alpha d)}. \tag{19}$$

The reflection is equal to the backward-traveling flux at x=*0,* divided by the incident flux $\Phi_0/4$,

$$R = \frac{I^-(0)}{\Phi_0/4} = 1 - 2\alpha D\coth(\alpha d). \tag{20}$$

Similarly, the transmission is the forward-traveling flux a *x=d* divided by the incident flux,

$$T = \frac{I^+(d)}{\Phi_0/4} = \frac{2\alpha D}{\sinh(\alpha d)}. \tag{21}$$

In terms of the μ_a and Λ, the reflection and transmission coefficients can be written as

$$R = 1 - 2\left(\frac{\mu_a \Lambda}{3}\right)^{1/2} \coth\left[\left(\frac{3\mu_a}{\Lambda}\right)^{1/2} d\right], \tag{22}$$

$$T = 2\left(\frac{\mu_a \Lambda}{3}\right)^{1/2} \operatorname{csch}\left[\left(\frac{3\mu_a}{\Lambda}\right)^{1/2} d\right]. \tag{23}$$

In the limit of no absorption, μ_a=0 and

$$R = 1 - \frac{2\Lambda}{3d} \quad \text{and} \quad T = \frac{2\Lambda}{3d}. \tag{24}$$

As a test of accuracy, we considered 424-nm Si spheres (with index 3.15) in air medium (index 1) at various volume loading densities (% v/v) and calculated T using Eq. 17 as a function of layer thickness. The calculated results, compared to calculations from *LightTools*, and are shown in Figure 8 at two values of loading density. We see that the theory agrees very well with the all-numerical method.

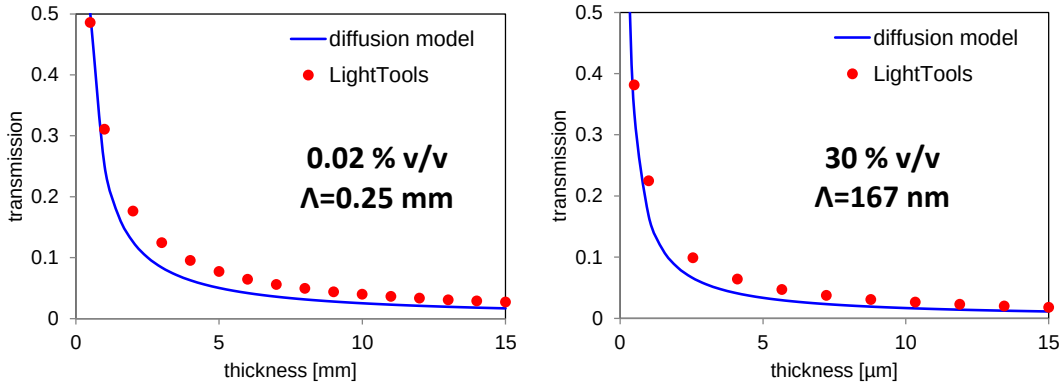

Figure 8. Comparison of T calculated by our diffusion model (line) with that obtained in *LightTools* software (dots).

For the above calculations, the required Λ (Eq. 10) is obtained from Mie scattering cross section by assuming an isolated sphere in the medium. This assumption is valid in the dilute loading case. For the diametrically opposite case in which only a few particles are missing in an otherwise ordered lattice of particles in a medium, we can use our recently developed GEM model (Section 2.1.2) and calculate the cross section and transmission.

2.2 Semi-Analytical (g-δ) Method

We wanted to develop a disorder theory for MMs with constituent materials of arbitrary shape, not just spheres, and with respect to different underlying lattice structures, not just simple cubes. Since an all-analytical solution for a general case is more difficult, we resorted to a semi-analytical solution.

2.2.1 Effective Medium

An analytical solution is possible for ordered arrangement of dielectric particles with ε_2 and μ_2 embedded in host materials with ε_1 and μ_1. The particles can be in different shapes (e.g., sphere, ellipsoid, cylinder, cube). They can also be arranged in a host material in a variety of ways: cubic (including simple, face-centered, and body-centered), hexagonal, tetragonal, orthorhombic, and others. A general scheme has been previously developed[16] to decouple contributions from particles and from their arrangement (or lattice structure) in the host. The effective dielectric constant can be written as

$$\hat{\varepsilon} = \varepsilon_1 \left[1 + \frac{4\pi}{\Omega} \hat{g} \left(1 + \frac{1}{\Omega} \hat{\delta} \hat{g} \right)^{-1} \right], \tag{25}$$

where g is the scattering matrix determined by an isolated particle, δ is the geometric matrix determined by the lattice (thus called g-δ approach), and Ω is the cell volume. Thus, the contributions from the particles and the lattice can be evaluated separately, which greatly simplifies the calculation of the effective dielectric constant. For spheres in a simple cubic lattice, this approach reduces to the Lewin[8] model.

We have implemented this approach to calculate the effective permittivity and permeability in more complex structures, such as spheres in a rectangular lattice and core-shells in a rectangular lattice. Figure 9a shows the effective ε and μ for spheres in a square lattice, in which the unit cell vector in x, y, and z directions (a, b, and c) are equal. Figure 9b displays the values for a rectangular lattice with $a=c$, $b=3a$. Notice that the symmetry in ε and μ is now broken with yy component differing from other two components. This is well captured in this approach.

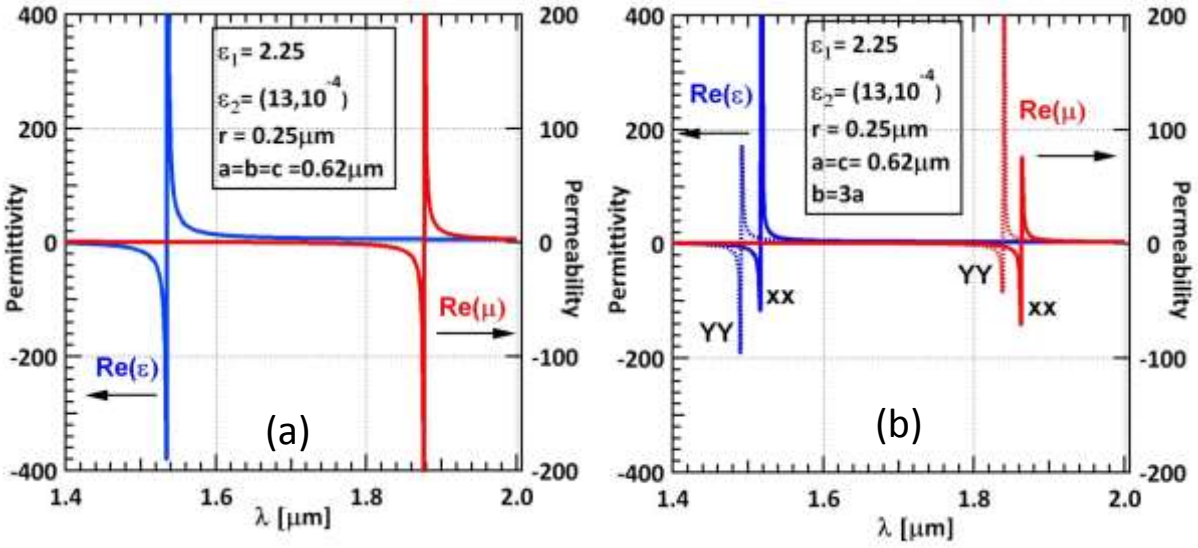

Figure 9. Wavelength-dependent effective permittivity(blue) and permeability (red) in (a) square lattice with *a=b=c*, and (b) rectangular lattice with *a=c*, *b=3a*.

2.2.2 Hybrid with HFSS

In the original *g*-δ approach, the scattering *g* matrix is obtained from the Mie solution of a single particle. In a metamaterial, since the particles are close together, the results from the *g*-matrix theory deviate from the exact results obtained from the HFSS. Indeed, for spheres in a simple cubic lattice, the HFSS results can be significantly different from those predicted by the Lewin model (as seen in an earlier section). In addition, closed-form expression for *g* is unavailable for shapes other than spheres. To overcome both limitations, we developed a hybrid *g*-δ approach.

The *g*-matrix theory can be improved by treating the g-matrix as a "renormalized" scattering matrix. First, we choose a lattice structure and shape of the constituent. Then, we obtain the effective ε and μ using HFSS. We adjust this renormalized *g*-matrix in our *g*-δ approach so that the obtained effective permittivity and permeability agree with the HFSS results. Now the disorder in the lattice, which affects only the δ matrix, can easily be evaluated. This approach is similar to the "quasi-particle" approach in solid-state theory, where the interaction between the electrons does not allow the free electrons theory to be applied. However, the interactions are included in renormalizing the mass of the electrons; the resulting quasi-particles are non-interacting (or mildly interacting), and thus simple theories can be applied. In our case, the *g*-matrix obtained to yield HFSS results includes major interactions between Mie scatters and thus enables us to study the disorder as a perturbation. This is critical to studying the disorder effect because it provides a common reference for future verification of our disorder theory by the HFSS for some controlled-disorder MMs.

We have developed a numerical code and successfully implemented this strategy.

2.2.3 Disorder: Isotropic

In this section, we consider the case of random disorder where the effective ε and μ can be treated as a product of a scalar and a unit matrix.

The hybrid approach described in the above section is then applied to study disorder. The procedure sequence is shown schematically in Figure 10. For the chosen volume fraction, we start with ordered composite, calculate δ and adjust *g* to reproduce HFSS value. Then, for the chosen disorder we calculate δ and use its *g*-δ formalism to get the effective parameters ε and μ. This calculation will be repeated for a number of disorder arrangements and their effective parameters will be appropriately averaged as described below.

In general, there are two kinds of disorder in metamaterials: (1) size disorder, which describes the fluctuation in particle sizes; and (2) location disorder, which describes the deviation in particle locations from their "supposed" places in an ordered structure. The physics and effects of size disorder are relatively easy to understand in terms of the local volume fluctuations, and so we focus on the location disorder, which does not alter the local volume fluctuation.

A disordered metamaterial can be viewed as a combination of many small ordered pieces whose lattice constants differ from one another. We assume that each small piece has a rectangular lattice with lattice constants of *a*, *b*, and *c*. The effective permittivity and permeability for each small piece can be calculated from the g-matrix theory with the renormalized g-matrix obtained by comparing with the HFSS results.

Then, we vary the lattice constants *a*, *b*, and *c*, but keep the unit-cell volume Ω=*abc* constant. The disorder strength is

$$\left\langle \delta\vec{r}_i \bullet \delta\vec{r}_j \right\rangle = \delta_{ij}\left[(\delta a_i)^2 + (\delta b_i)^2 + (\delta c_i)^2\right] = \delta_{ij}\Delta^2 \tag{26}$$

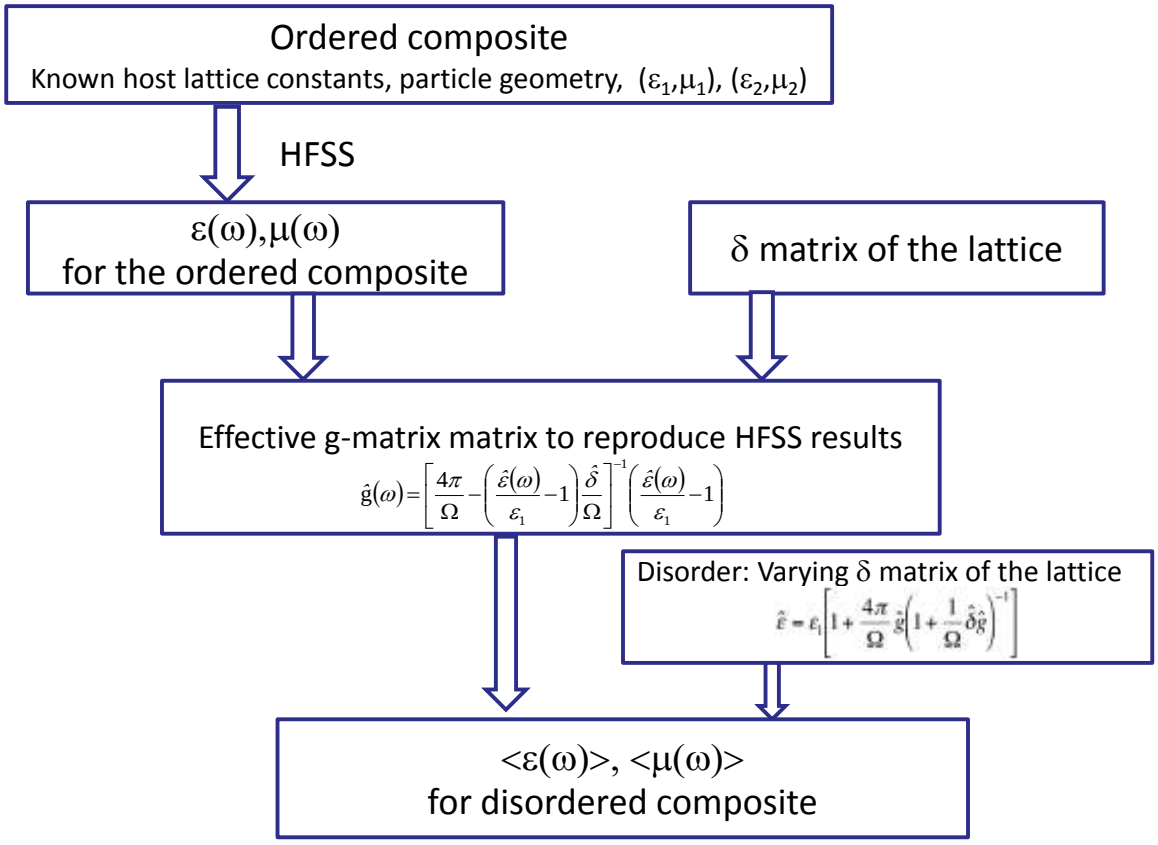

Figure 10. Outline of disorder calculations.

and the relative disorder strength is defined as

$$\gamma = \Delta/a_0 \tag{27}$$

and a_0 is the lattice constant of the ordered cubic structure.

The effective permittivity and permeability of the whole system is then obtained by averaging over the small pieces. However, caution must be taken when averaging the permittivity and permeability. From the Maxwell equation, the local-field change and the dielectric variation are related. Consequently, the averaged dielectric constant in the presence of fluctuations is

$$\tilde{\epsilon}_x = \epsilon_x - \frac{1}{3\epsilon_x}\overline{(\delta\epsilon_x)^2} \tag{28}$$

or equivalently,

$$\tilde{\epsilon}_x^{1/3} = \overline{\epsilon^{1/3}} \tag{29}$$

Explicitly, we choose a value of γ, then consider a distribution (denoted as *m*) of the constituents, and calculate ε_m and μ_m for that configuration. We consider a number of distributions subject to the condition that the lattice constant *a* lies between $a_0(1-\gamma)$ and $a_0(1+\gamma)$ and calculate ε_m and μ_m for each of the configurations. The average value of the effective ε and μ is simply the average of $\varepsilon_m^{1/3}$ and $\mu_m^{1/3}$, as given in Eq. 29.

The code has been developed, and for demonstration we have applied it to two cases: high contrast with ε_2=50 and ε_1=1; and low contrast with ε_2=12 and ε_1=1. The calculated results for the high-contrast case are shown in Figure 11. The effective ε for the ordered lattice (Figure 11a, solid black line) as a function of a/λ shows an anti-resonance near 0.18 and a full resonance near 0.24. Figure 11a (right axis) also shows the calculated deviation in ε from its ordered lattice value for various values of γ: γ=0.05 (cyan), 0.10(green), and 0.15 (red). We see that the difference is largest only near the resonance and increases with disorder as expected. Although the change in ε value is large, the calculated reflectivity (Figure 11b) from a thin layer of MM exposed to air on both sides changes minimally (less than 0.3) and only near the resonance.

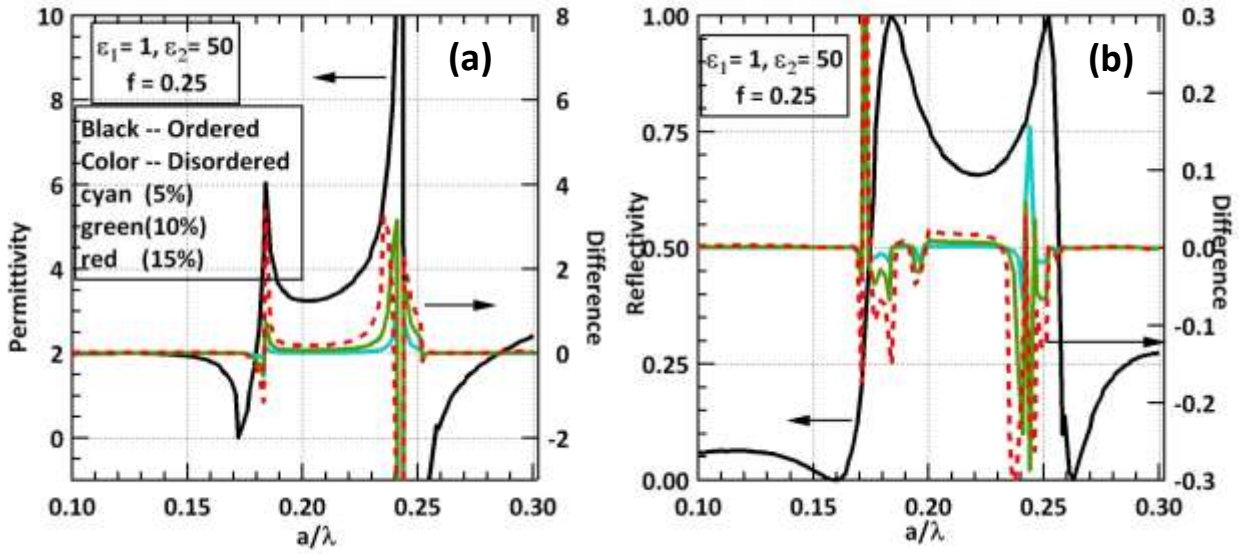

Figure 11. Effect of location disorder on (a) permittivity and (b) reflectivity for the MM with high contrast constituent as indicated. The solid black line denotes the value calculated for ordered arrangement (read off the left axis). The colored lines denote the difference (read off the right axis) between the values obtained for disordered arrangement and ordered arrangement. The relative disorder strengths γ of 5%, 10%, and 15% are considered.

Results of similar calculations with low-contrast spheres (ε_2=12) in air (ε_1=1) are shown in Figure 12a (permittivity) and Figure 12b (reflectivity). As before, the effect of disorder is largest near the resonance (and anti-resonance) and generally increases with disorder. We note that the effect of disorder on the reflectivity near the resonances is much larger in this case compared to that in the high-contrast case. When the dielectric contrast is large, the Mie resonance is well-contained within the sphere and can be treated as a collection of noninteracting spheres. The effective materials parameter is less dependent on the arrangement. However, in the low-contrast case, the Mie modes are leaky and interact with the modes from the neighbors. Hence, the

disorder arising from the deviation in lattice arrangement has a larger effect on the effective parameters and reflectivity, as indicated in Figure 12.

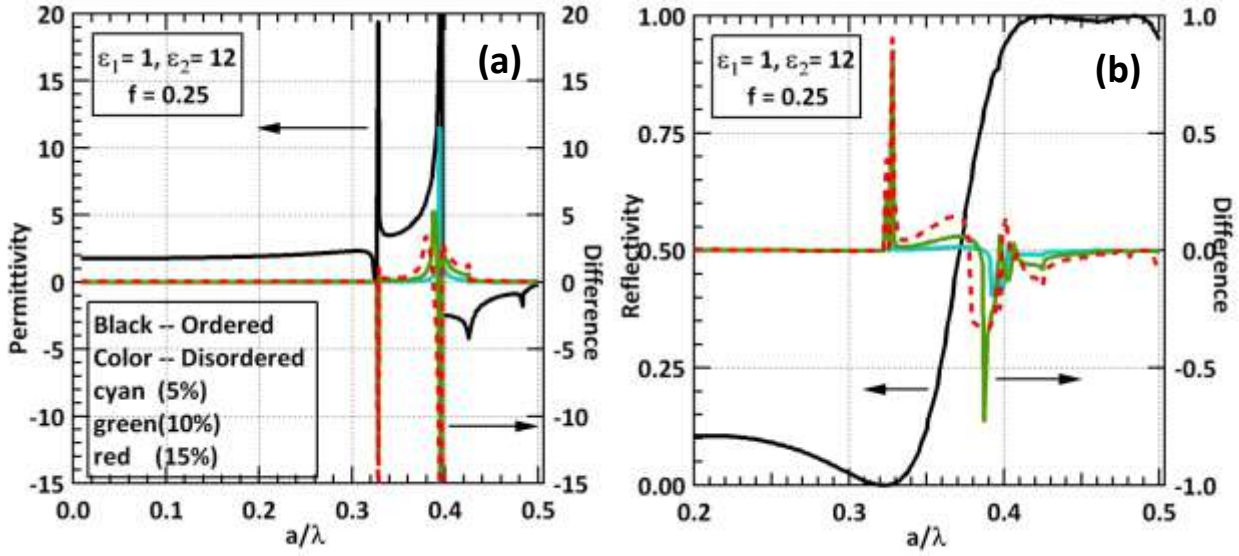

Figure 12. Effect of location disorder on (a) permittivity and (b) reflectivity for the MMs with low-contrast constituent as indicated. The solid black line denotes the value calculated for ordered arrangement (read off the left axis). The colored lines denote the difference (read off the right axis) between the values obtained for disordered arrangement and ordered arrangement. The relative disorder strengths γ of 5%, 10%, and 15% are considered.

In summary, we have developed a hybrid-analytical approach to study disorder in MMs. This approach can in principle be applied to MMs with constituent particles of arbitrary shape and various underlying lattices. In the following section, we have further extended the approach to controlled disordered systems. This theory will establish the relation between the effective permittivity and permeability and the individual particles' locations and sizes.

2.2.4 Disorder: Anisotropic

In this section we consider the case of controlled disorder, where the effective ε and μ are general matrices with unequal diagonal elements and non-zero off-diagonal elements. To the best of our knowledge, the concept of the local anisotropy caused by disorder has not yet been considered for MMs.

Designing novel metamaterials for important applications relies on finite-element tools such as HFSS, which can model only perfect ordered structures—typically particles arranged in a simple cubic structure. For practical applications with reasonable cost, the fabricated structures inevitably contain many imperfections compared with the design. It is important to understand and quantify the effect of these imperfections (disorder) on the materials' optical properties.

Even in the regions where the effective-medium approximation is acceptable, an adequate description of disorder proves to be challenging. The ordered structures commonly studied are simple cubic, which is isotropic, and the effective ε and μ can be described by a scalar. In the presence of disorder, particularly location disorder, the system is locally anisotropic. Using a

"modified" scalar to describe the disorder effect would underestimate, or even completely miss, the disorder effect. To the best of our knowledge, the concept of the local anisotropy caused by disorder has not yet been considered for MMs.

We have developed our theory based on the g-δ method to evaluate the effect of both size and location disorder on dielectric and optical properties of MMs. Below we provide the outline and show that both specular reflection and diffused scattering work within the effective-medium framework.

First, we consider size disorder in a system with sphere inclusions. A perfect structure is achieved by arranging identical spheres in a simple cubic lattice. Disorder in such a system falls into two categories: fluctuation in particle size and fluctuation in location. For size disorder, the underlying lattice structure remains cubic, and therefore, the effective ε and μ are still isotropic. The effective ε and μ certainly will depend on the fluctuation because different particle sizes would give rise to Mie resonances at different frequencies. The effect of size disorder can be readily evaluated by using the *g*-δ approach. We follow the original derivation of the *g*-δ formalism (described in Section 2.2.1) and apply it to a system with size disorder. In brief, for an ordered structure, after including the Mie scattering of individual particles, the Maxwell equations for local averaged E and H can be expressed as

$$\begin{aligned} \nabla\times\mathbf{E} &= -ik\mu_1\left[1+\frac{4\pi}{\Omega}\hat{p}\left(1+\frac{1}{\Omega}\hat{\delta}\hat{p}\right)^{-1}\right]\mathbf{H} \\ \nabla\times\mathbf{H} &= ik\varepsilon_1\left[1+\frac{4\pi}{\Omega}\hat{g}\left(1+\frac{1}{\Omega}\hat{\delta}\hat{g}\right)^{-1}\right]\mathbf{E} \end{aligned}, \tag{30}$$

where g and p are the Mie coefficients for electric and magnetic resonance of an isolated particle (controlled by the particle radius) and δ is the geometry factor (controlled solely by the lattice). Thus the effective ε and μ for an ordered structure are

$$\begin{aligned} \varepsilon &= \varepsilon_1\left[1+\frac{4\pi}{\Omega}\hat{g}\left(1+\frac{1}{\Omega}\hat{\delta}\hat{g}\right)^{-1}\right] \\ \mu &= \mu_1\left[1+\frac{4\pi}{\Omega}\hat{p}\left(1+\frac{1}{\Omega}\hat{\delta}\hat{p}\right)^{-1}\right] \end{aligned} \tag{31}$$

$$\begin{aligned} &\hat{g}=\frac{a^3}{Q}\hat{1}, \qquad \hat{p}=\frac{a^3}{P}\hat{1}, \qquad Q=\frac{\varepsilon_p+2\varepsilon_1}{\varepsilon_p-\varepsilon_1} \qquad P=\frac{\mu_p+2\mu_1}{\mu_p-\mu_1} \\ &\frac{\varepsilon_p}{\varepsilon_2}=\frac{\mu_p}{\mu_2}=F\left(ka\sqrt{\varepsilon_2\mu_2}\right), \qquad F(x)=\frac{2(\sin x-x\cos x)}{(x^2-1)\sin x+x\cos x} \end{aligned}. \tag{32}$$

In the presence of size disorder, we find a similar *g*-δ expression can be obtained, with the *g* and *p* matrices replaced by their averaged over different sizes.

$$\hat{g} \to \bar{\hat{g}}, \hat{p} \to \bar{\hat{p}}$$
$$\bar{\hat{g}} = \frac{1}{N}\sum_i \frac{a_i^3}{Q_i}\hat{1} \qquad \bar{\hat{p}} = \frac{1}{N}\sum_i \frac{a_i^3}{P_i}\hat{1} \quad . \tag{33}$$

Figure 13 compares our theoretical results with HFSS simulations and shows that size disorder can change resonance structures, which is understandable because the Mie resonance is controlled by the particle size.

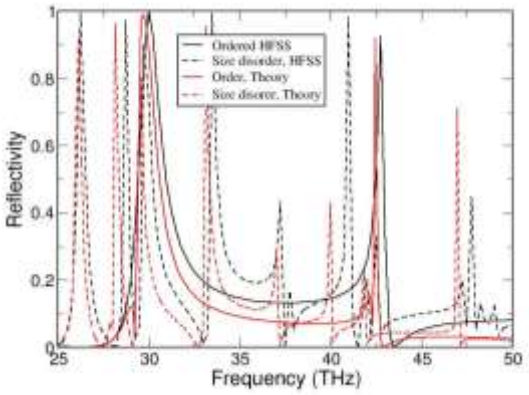

Figure 13. Effect of size disorder on reflection.

We see that the modified g-δ theory with disorder effect included agrees with the HFSS simulations reasonably well, and therefore captures the essential physics. Some slight discrepancy is due to the fact that the g-δ theory starts from the Lewin model and is inaccurate for the ordered case as compared to the HFSS. The major effect of size disorder is that a major resonance splits into many small resonances.

In the case of location disorder, the particles are the same size but are not on ordered cubic lattice sites. This disorder has not been systematically considered in the literature. In fact, most effective-medium theories, where the effective ε and μ depend on only loading and particle size, would predict that location disorder has no effect on optical properties of composite materials. However, experimental measurements clearly demonstrate a strong effect of location disorder on reflection and transmission of a composite. We notice that in the presence of location disorder, the perfect cubic structure is disturbed and becomes anisotropic locally. The anisotropy has a profound effect on light propagation and cannot be captured by an effective isotropic ε and μ.

One effect is that light propagation along different directions would have different wave numbers, which in turn alters light polarization, reflection, and transmission. While light propagation in anisotropic crystals has been studied in literature, only either ε or μ were considered to be anisotropic. The location disorder here would render both ε and μ anisotropic. Thus we must start from the fundamental Maxwell equations and derive a theory for this case.

The Maxwell equations for monochromic electromagnetic wave read

$$\nabla \times \mathbf{E} = -i\omega\mathbf{B}, \qquad \nabla \times \mathbf{H} = i\omega\mathbf{D} \tag{34}$$

Consider light propagation along the z-axis (normal incidence) and assume that location disorder occurs in the x-y plane. Hence the anisotropy is in the x-y plane. The permittivity and permeability tensors as well as the obtained Helmholtz equations are

$$\boldsymbol{\varepsilon} = \begin{pmatrix} \varepsilon_{xx} & \varepsilon_{xy} \\ \varepsilon_{xy} & \varepsilon_{yy} \end{pmatrix}, \qquad \boldsymbol{\mu} = \begin{pmatrix} \mu_{xx} & \mu_{xy} \\ \mu_{xy} & \mu_{yy} \end{pmatrix}$$

$$\nabla \times \left[\nabla \times \begin{pmatrix} H_x \\ H_y \end{pmatrix} \right] = \omega^2 \begin{pmatrix} \varepsilon_{yy}\mu_{xx} - \varepsilon_{xy}\mu_{xy} & \varepsilon_{yy}\mu_{xy} - \varepsilon_{xy}\mu_{yy} \\ \varepsilon_{xx}\mu_{xy} - \varepsilon_{xy}\mu_{xx} & \varepsilon_{xx}\mu_{yy} - \varepsilon_{xy}\mu_{xy} \end{pmatrix} \begin{pmatrix} H_x \\ H_y \end{pmatrix} \tag{35}$$

$$\nabla \times \left[\nabla \times \begin{pmatrix} E_x \\ E_y \end{pmatrix} \right] = \omega^2 \begin{pmatrix} \varepsilon_{xx}\mu_{yy} - \varepsilon_{xy}\mu_{xy} & \varepsilon_{xy}\mu_{yy} - \varepsilon_{yy}\mu_{xy} \\ \varepsilon_{xy}\mu_{xx} - \varepsilon_{xx}\mu_{xy} & \varepsilon_{yy}\mu_{xx} - \varepsilon_{xy}\mu_{xy} \end{pmatrix} \begin{pmatrix} E_x \\ E_y \end{pmatrix}$$

For normal incidence, the electric field can be written as

$$\mathbf{E} = \begin{pmatrix} E_x \\ E_y \end{pmatrix} e^{ikz - i\omega t} \tag{36}$$

The eigenvalues of k can be obtained by the equation

$$\det \begin{pmatrix} k^2 - \dfrac{\omega^2}{c^2}u & -\dfrac{\omega^2}{c^2}v \\ -\dfrac{\omega^2}{c^2}v & k^2 - \dfrac{\omega^2}{c^2}u \end{pmatrix} = 0, \qquad \begin{aligned} u &= \varepsilon_{xx}\mu_{yy} - \varepsilon_{xy}\mu_{xy} \\ v &= \varepsilon_{xy}\mu_{yy} - \varepsilon_{yy}\mu_{xy} \end{aligned} \tag{37}$$

This equation gives rise to two distinct eigenvalues k_α and k_β

$$k^2_{\alpha(\beta)} = \frac{\omega^2}{c^2}\left[u + (-)v\right], \tag{38}$$

with corresponding eigenvectors

$$\left(\mathbf{E}^\alpha, \mathbf{E}^\beta\right) = \begin{pmatrix} \cos\phi & -\sin\phi \\ \sin\phi & \cos\phi \end{pmatrix}. \tag{39}$$

It is clear that the location disorder can create local anisotropy in the material. We will now establish a quantitative relation between local anisotropy and disorder before calculating the effect of disorder on reflection and transmission of a metamaterial. We start from the fundamental dielectric theory. The dielectric response at a given particle ultimately comes from all other dipoles in the system. Since the electric field created by a dipole is

$$\mathbf{E} = -\frac{1}{4\pi\varepsilon_{00}}\left[\frac{\mathbf{p}}{r^3} - \frac{3(\mathbf{p}\bullet\mathbf{r})\mathbf{r}}{r^5}\right], \tag{40}$$

where ε_{00} is the vacuum dielectric constant, the total electric field by all these dipoles is

$$\mathbf{E}_s = T \bullet \mathbf{p} \tag{41}$$

$$T = \frac{1}{4\pi\varepsilon_{00}} \begin{pmatrix} \sum \dfrac{3x^2 - r^2}{r^5} & \sum \dfrac{3xy}{r^5} \\ \sum \dfrac{3xy}{r^5} & \sum \dfrac{3y^2 - r^2}{r^5} \end{pmatrix}. \tag{42}$$

In a simple cubic structure, the off-diagonal term will be zero due to the inversion symmetry. However, when location disorder is present, the off-diagonal element becomes finite. Since the off-diagonal term decays with the distance quickly, only the surrounding dipoles' contribution is important. If we retain only the nearest-neighbor dipoles, we obtain

$$T_{xy} \approx -\frac{5}{a^3}\sum_{i=1}^{4}\frac{(x_i - x_0)(y_i - y_0)}{a^2} \tag{43}$$

where *a is* the unit-cell size of the ordered cubic structure, (x_i,y_i) are the coordinates of the surrounding particles, and (x_0,y_0) is the location of interest. The polarization at this point is proportional to the total field (applied and induced fields),

$$\mathbf{p} = \alpha(\mathbf{E}_0 + \mathbf{E}_s) = R^{-1}\mathbf{E}_0, \tag{44}$$

where α is the polarizability of the particle, and the matrix *R* is

$$R = \begin{pmatrix} T_{xx} - \alpha^{-1} & T_{xy} \\ T_{xy} & T_{yy} - \alpha^{-1} \end{pmatrix}, \tag{45}$$

with its inverse

$$R^{-1} \approx \begin{pmatrix} \left(T_{xx} - \alpha^{-1}\right)^{-1} & -T_{xy}/\left[\left(T_{xx} - \alpha^{-1}\right)\left(T_{yy} - \alpha^{-1}\right)\right] \\ -T_{xy}/\left[\left(T_{xx} - \alpha^{-1}\right)\left(T_{yy} - \alpha^{-1}\right)\right] & \left(T_{yy} - \alpha^{-1}\right)^{-1} \end{pmatrix}. \tag{46}$$

The dielectric tensor is

$$\varepsilon = 1 - \frac{N}{\varepsilon_{00}} R^{-1}, \tag{47}$$

where *N* is the number of particles per unit volume. If we further assume that T_{xy} is much smaller than T_{xx}, we obtain the diagonal dielectric constant,

$$\varepsilon_0 = 1 + \frac{N\alpha/\varepsilon_{00}}{1 - \alpha T_{xx}}, \tag{48}$$

and the off-diagonal element,

$$\varepsilon_{xy} = -(\varepsilon_0 - 1)^2 T_{xy} = -\frac{15\gamma}{\pi}(\varepsilon_0 - 1)^2, \tag{49}$$

where the parameter γ,

$$\gamma = \frac{1}{4}\sum_{i=1}^{4}\frac{(x_i - x_0)(y_i - y_0)}{a^2}, \tag{50}$$

quantifies the local location disorder.

Thus, having established the relation between the off-diagonal dielectric response ε_{xy} and the location disorder, we can calculate the reflection and transmission for a known disordered arrangement.

First, we consider reflection from a semi-infinite MM surface located at $z>0$. The polarization of incident light is assumed to be along the x-axis,

$$\begin{cases} \left(e^{ik_1 z}, 0, 0\right) & \text{Incident} \\ \left(re^{-ik_1 z}, r' e^{-ik_1 z}, 0\right) & \text{reflected} \\ \left(t_\alpha \mathbf{E}^\alpha e^{ik_\alpha z} + t_\beta \mathbf{E}^\beta e^{ik_\beta z}, 0\right) & \text{transmitted} \end{cases} \tag{51}$$

Because of the anisotropy, the electric field of the reflected (transmitted) light has components along both the x- and y-axes. In other words, the location disorder can specularly scatter light from the "S" polarized to the "P" polarized state, and vice versa.

Across the interface $z=0$, both the electric field **E** and magnetic field **H** in the lateral direction are continuous, which give rise to the following boundary conditions

$$\begin{cases} 1+r = t_\alpha E_x^\alpha + t_\beta E_x^\beta \\ r' = t_\alpha E_y^\alpha + t_\beta E_y^\beta \\ k_1(1-r) = \dfrac{1}{\mu_0}\left(k_\alpha t_\alpha E_y^\alpha + k_\beta t_\beta E_y^\beta\right) + \dfrac{\mu_{xy}}{\mu_0^2}\left(k_\alpha t_\alpha E_x^\alpha + k_\beta t_\beta E_x^\beta\right) \\ -k_1 r' = \dfrac{\mu_{xy}}{\mu_0^2}\left(k_\alpha t_\alpha E_y^\alpha + k_\beta t_\beta E_y^\beta\right) + \dfrac{1}{\mu_0}\left(k_\alpha t_\alpha E_x^\alpha + k_\beta t_\beta E_x^\beta\right) \end{cases} \tag{52}$$

where to simplify the expressions, we assume $\mu_0=\mu_{xx}=\mu_{yy}$ and $\varepsilon_0=\varepsilon_{xx}=\varepsilon_{yy}$. Solving these equations we obtain

$$r = \frac{1-\xi^2+\eta^2}{(1+\xi)^2-\eta^2} \qquad r' = -\frac{2\eta}{(1+\xi)^2-\eta^2} \tag{53}$$

$$\xi = \sqrt{\frac{\varepsilon_0}{\mu_0}} \qquad \eta = \frac{1}{2}\sqrt{\frac{\varepsilon_0}{\mu_0}}\left(\frac{\varepsilon_{xy}}{\varepsilon_0} + \frac{\mu_{xy}}{\mu_0}\right). \tag{54}$$

Note that k_α and k_β in Eq. (53) depend on ε_{xy}, as shown in Eq. (38), which is why Eqs. (53) and (54) contain ε_{xy},

Clearly we see that in the presence of disordered-induced anisotropy, the reflected light has a finite component along the y-axis. Thus the polarization of light rotates after it is reflected by such anisotropic materials. This effect cannot be captured by an isotropic effective medium.

The total reflection coefficient should be

$$R = |r|^2 + |r'|^2, \tag{55}$$

which also depends on η due to the anisotropy.

Figure 14 plots the reflection spectrum and its dependence on the disorder strength. The ordered structure is designed to achieve perfect reflection over a large range of frequency. At small disorder, the reflection along the same polarization direction as the incident light is reduced as

compared to the ordered structure. However, the total reflection does not seem to change much. Thus the main effect of a small disorder is change in the polarization direction. As the disorder strength increases, not only does the reflection along the polarization direction of the incident light decrease considerably, but also the total reflection, because as the disorder-induced anisotropy increases, the Mie resonance structure changes. Mathematically, the large off-diagonal ε_{xy} and μ_{xy} shift the poles in the determinant of ε and μ considerably.

In practice, the MMs are only a few layers thick and very rarely form a semi-infinite surface. Hence we consider the reflection from a slab MM. In most experiments and applications, the metamaterial is a thin slab located between $z=0$ and $z=-\Delta$. The incident, reflected, and transmission light as well as the light inside the slab can be expressed as:

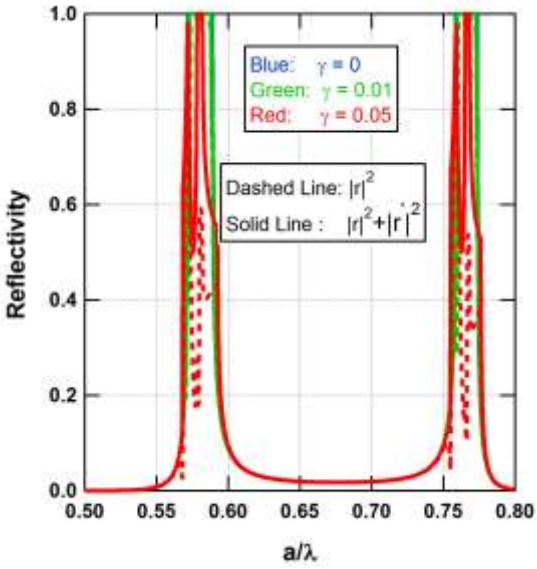

Figure 14. Reflectivity as a function of a/λ for a semi-infinite MM with different disorder strengths. Dashed and solid lines correspond to reflection along the same polarization direction as the incident light and the total reflection. Here, a is the lattice constant of an ordered simple cubic structure, λ is the wavelength, and γ is the disorder strength.

$$\begin{cases} \left(e^{ik_1 z},0,0\right) & \text{incident} \\ \left(re^{-ik_1 z},r'e^{-ik_1 z},0\right) & \text{reflected} \\ \left(\left(c_\alpha e^{ik_\alpha z}+d_\alpha e^{-ik_\alpha z}\right)\mathbf{E}^\alpha+\left(c_\beta e^{ik_\beta z}+d_\beta e^{-ik_\beta z}\right)\mathbf{E}^\beta,0\right) & \text{in}-\text{slab} \\ \left(te^{ik_2(z-\Delta)},t'e^{ik_2(z-\Delta)},0\right) & \text{transmitted} \end{cases} \tag{56}$$

where we have eight unknown coefficients, which will be fixed by the boundary conditions at the two interfaces $z=0$ and $z=-\Delta$. We have obtained explicit expressions of r, r', t, and t', which are tedious and not shown here. Again, the total reflection is $|r|^2+|r'|^2$ and $|t|^2+|t'|^2$.

We computed the reflection and transmission spectra for different disorder strengths and plotted them in Figures 15 and 16, where we see that the reflection of this slab exhibits similar features to that of a half-infinite metamaterial. This can be readily understood: The perfect reflection region has a strong Mie resonance, and the light inside the metamaterial becomes highly evanescent. When the penetrating length of the evanescent wave is shorter than the slab thickness, the evanescent wave cannot sense any difference between the slab and the half-infinite bulk. Figure 16 plots the transmission spectra of the slab with different disorder strength. We see that any reduction in reflection in Figure 15 can be essentially accounted for from an enhancement in transmission, as expected because the material is non-absorbing.

Recently Professor Valentine's group (collaborator, Vanderbilt University) has fabricated several structures with controlled location disorder. Our theory explains the overall features of the

measurements. As noted earlier, the input for the g-δ theory is the effective ε and μ the constituent shapes in an ordered lattice. Since we had used in Figures 14-16 the input values as given by the less applicable Lewin's theory, we have not yet reproduced the measured reflection spectra of the ordered structures. However, when we used the input values obtained from HFSS methods, our reflectivity results for controlled disorder MMs compared well with those obtained from Vanderbilt measurements.

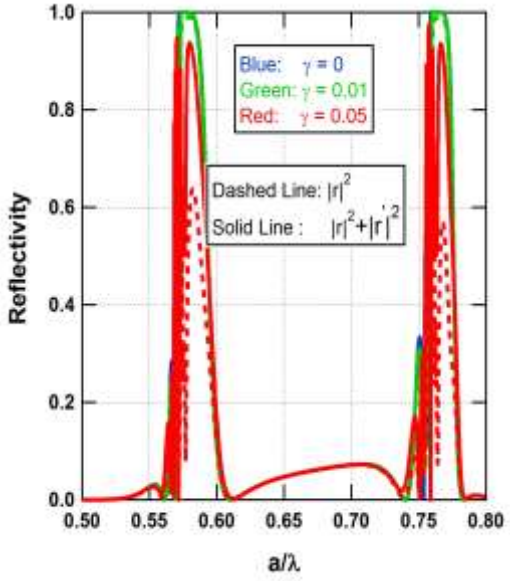

Figure 15. Reflectivity as a function of a/λ for a metamaterial slab with different disorder strengths.

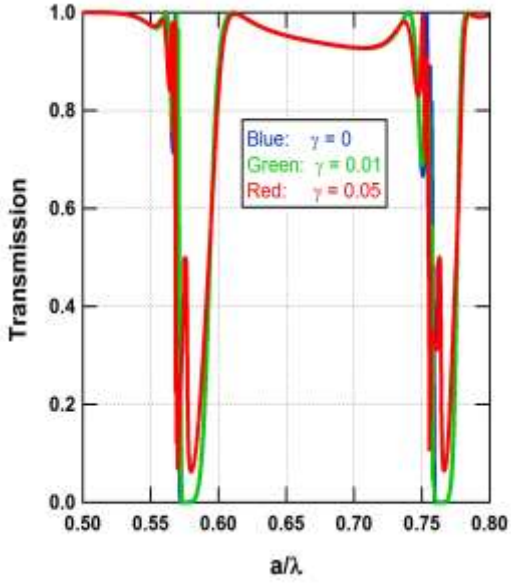

Figure 16. Transmission as a function of a/λ for the same metamaterial slab as in Figure 15.

So far we have considered only specular reflection and calculated the change arising from the off-diagonal element created by location disorder. Interestingly, the other component—diffused reflection or scattering—can also be calculated from the off-diagonal permittivity matrix elements $\delta\varepsilon_{ij,}$ by consider this as a Rayleigh-like scattering. Then, scattered radiation will have an angle distribution of $\sin^2\theta$, and is distinct from the specular reflection and transmission discussed above.

For the known distribution of location disorder, $\delta\varepsilon_{ij}$ will be calculated as stated above and then averaged over a number of distributions to get $\left\langle \delta\varepsilon_{ik}^2 \right\rangle$. The extinction coefficient α_R due to the Rayleigh-like scattering is then

$$\alpha_R = \frac{\omega^4}{18\pi c^4} V \left\langle \delta\varepsilon_{ik}^2 \right\rangle \tag{57}$$

$$\left\langle \delta\varepsilon_{ik}^2 \right\rangle = \frac{225}{16\pi^2}\left(\varepsilon_0 - 1\right)^4 \left\langle \left(x_i - x_0\right)^2 \left(y_i - y_0\right)^2 \right\rangle. \tag{58}$$

3. Applications

We applied the above developed theory of metamaterials to obtain the effective permittivity and permeability of all-dielectric structures. We exploited the Mie resonance-induced changes to the permittivity and permeability to study three applications, as discussed below.

3.1 Perfect Reflection

The enhanced reflection is one of the first applications we considered. Since our theory helped us to develop a fundamental physical understanding of the observed reflectance from MM surfaces, we fine-tuned the materials selection and the sizes and periodicity of Mie scatterers to achieve near-perfect reflection. A compact, nonabsorbing, perfectly reflecting layer would have numerous important applications—from bioimaging and nanosensing to improving laser efficiency to protecting the assets from laser damage. In particular, the Navy's counter-directed energy weapon (C-DEW) program can benefit from such surfaces.

We have used the commercial finite-element solver HFSS (ANSYS) to study the intrinsic and extrinsic properties of dielectric microparticles in a medium. By exploiting the Mie resonance in dielectric shapes, we designed a metamaterial monolayer made of Si short cylinders on silica surface to obtain extremely high reflectivity and negligible absorptivity. In contrast to Bragg reflectors and photonic band gap materials, which require multiple layers for high reflection, our single-negative metamaterial is highly reflective and sub-wavelength in thickness. The Vanderbilt group fabricated the surface and measured the reflection spectra, as shown in Figure 17 (a-c).

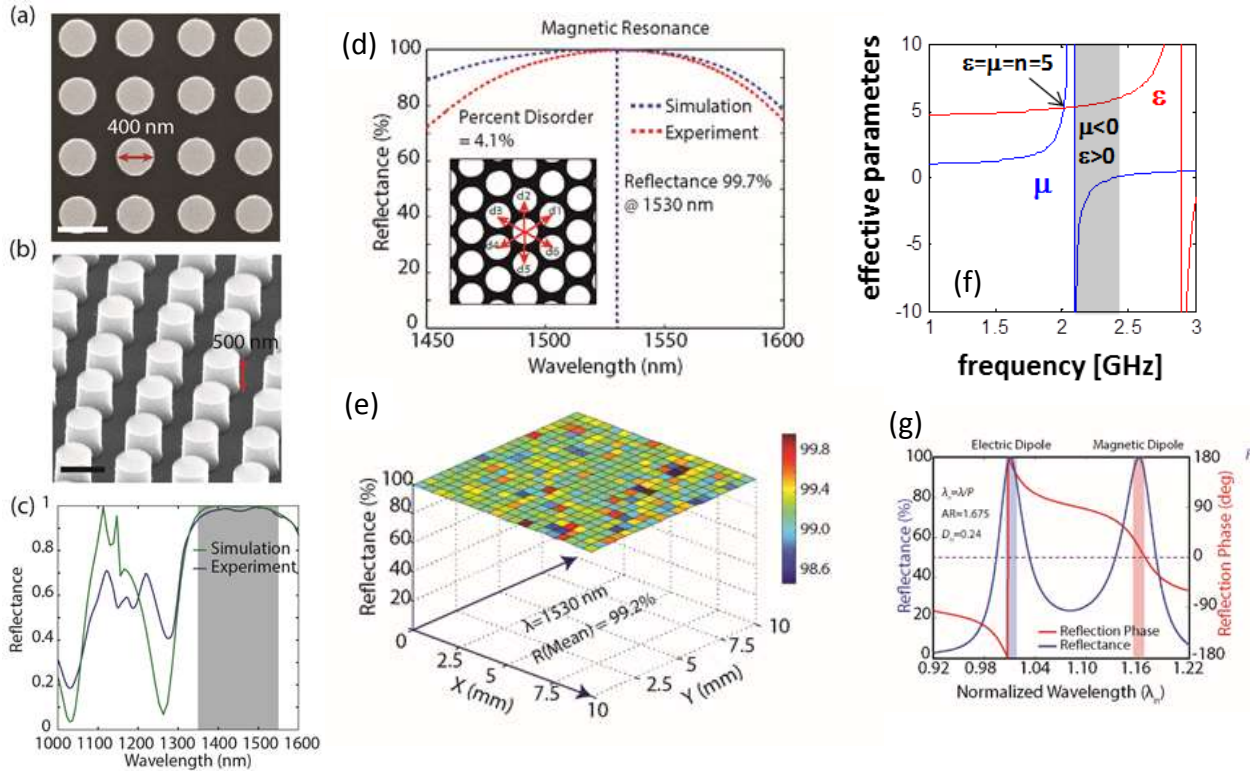

Figure 17. Measured reflection spectra from the sample fabricated by lithography (a-c) and large-area RIE (d, e). The MM structure is Si short cylinders on silica substrate. Our approach to reducing the antenna size and achieving an electrically resistive and magnetically conducting metasurface are shown in (f) and (g).

The samples were first fabricated by the lithographic approach (SEM pictures in Figure 17a and b) which is applicable for small-area samples. The measured and predicted reflection spectra are shown in Figure 17c. We then fabricated by reactive-ion etch (RIE) for large-area samples. Notice that very high reflection is obtained and in agreement with the predicted values. (Figure 17d). The larger discrepancy in the middle panel arises from the unintentional disorder in the self-assembly approach. In spite of the disorder, we note that reflection in excess of 98.6% is obtained across the cm x cm sample area (Figure 17e).

3.2 Short-Antenna and Magnetic Ground Plane

Two other useful properties of our metamaterial are shown in Figure 17f and 17g. It is possible to design the MM so that the effective ε and μ are equal and large at the chosen frequency. Figure 17f is for a design at 2 GHz with BST spheres in polymer. Since e=n=5, the effective index is 5, which allows a reduction in the size of the linear antenna from this material by a factor of 5. Since ε=μ, the impedance is 1 and is matched to that of free space. Consequently, the radiation from this antenna is full and complete while maintaining a much smaller size. For example, the size reduction will be 25 for a patch antenna, thus considerably reducing the antenna array size. Because of the small bandwidth, this concept is more useful for communication applications.

The second useful feature is the magnetic mirror. The shaded region (Figure 17f) just beyond the magnetic resonance is where $\mu<0$ and $\varepsilon>0$. In this region, the metamaterial is a perfect reflector, as discussed before. However, in contrast with a conventional metallic mirror in which E field is zero at the surface, here the H field on the surface is zero. In addition, as illustrated in Figure 17g, the phase shift in reflection from the magnetic reflector is zero. Note the wavelength is normalized to that electric resonance wavelength of the device fabricated in Figure 17d. These properties enable: (a) the placement of antenna directly on the surface without the need for a quarter-wavelength layer, as in the case of an electrical conductor; (b) an increase in the directivity because the antenna's image is not reversed; and (c) reduced or eliminated interference from the surface currents generated by the incident radiation. This metasurface can be designed for the chosen compact antenna frequency.

3.3 Polarizer

Our analytical theory, which treats each constituent as electric or magnetic dipole and adds the contribution from all neighbors, arrives at an effective dielectric tensor for the metamaterial. It helps us understand the origin of anisotropic permittivity and permeability in MMs arising from isotropic constituents. The Mie scattering constituents can be placed in a controlled disordered arrangement to achieve tensor (ε and μ) with unequal diagonal elements and vanishing off-diagonal elements or with equal diagonal elements and non-zero off-diagonal elements. In the former case, we get a polarizer and the in latter case we get a polarization rotator. For example, Figure 18a shows the polarization-dependent reflectivity by an anisotropic array of Si cylinders (inset). The calculations indicate nearly 100% transmission at 1.5 μm for y- polarized light and 100% reflection for x-polarized light. For x-polarized light, the interaction between spheres along the x direction is enhanced because the spheres are close together, causing the electric and magnetic Mie resonances of the cylinder to coalesce and form a broad bandwidth of high reflectivity[3]. On the other hand, for y-polarized light the interaction between cylinders is weak

because their separation in the y direction is large, causing the resonances to separate spectrally and weaken, resulting in low reflectivity. The permittivity tensor calculated for this structure with our theory clearly shows different diagonal components corresponding to x and y polarizations. This physics-based theory, currently being written up for publication, enables us to develop efficient submicron-thick polarizers.

In an independent study, the Vanderbilt group fabricated[17] structurally anisotropic constituents on isotropic lattice silicon unit cells (Figure 18b)—which is complementary to the SRI design discussed above—and demonstrated near-unity polarization conversion over a 200-nm bandwidth (Figure 18c). However, one drawback of such metasurfaces is that they must operate in reflection mode to achieve this large bandwidth.

Figure 18. (a) Anisotropic unit cell and predicted spectral reflectivity for x-polarized (black) and y-polarized (red) light by a single layer of Si cylinders with radius of 0.2 μm, a_x=0.7 μm, and a_y=1.23 μm. Near 1.5 μm, light polarized along x is 100 % reflected and light polarized along y is nearly fully transmitted. (c) Schematic of structurally anisotropic metasurface for polarization conversion. (d) Polarization conversion efficiency vs. wavelength. Note that this metasurface operates in reflection.

4. Conclusions and Recommendations

SRI recommends that further studies to be conducted to take advantage of the knowledge base created under the current program. In particular:

(a) *Shapes other than spheres.* We have developed formalism that obtains the effective frequency-dependent permittivity and permeability of the composite metamaterial if those of the constituents are known. This formalism allows us to achieve an all-analytical method if the shapes are spherical where the analytical form of constituent parameters is available by Lewin or GEM. For nonspherical shapes, the formalism allows us to use all-numerical constituent parameters obtained in accurate numerical methods (for example, HFSS). In the current program, we have tested our formalism only for spherical shapes. Application to other shapes is straightforward and when completed will enable us to explore a much larger design space for a number of applications.

(b) *Thin-film polarizer.* The submicron-thick silicon-based anisotropic structures are compatible with optoelectronic devices and integrated photonic circuits. By avoiding the use of metals, these surfaces allow low-loss operation and, for large incident intensities, overcome thermal limitations of thin-film polymer polarizers. Unlike other inorganic thin-film polarizers, the metamaterials polarizer does not require birefringent materials or

operation at the Brewster angle. As discussed in Section 3.3, the metamaterial can be designed to have submicron thickness and near total polarization-dependent reflection and transmission. Such designs should be fabricated, tested, and used in the applications. A similar design should be developed to rotate the polarization upon transmission and/or reflection. Our preliminary designs show such a possibility. However, the designs will have to be optimized for near-perfect conversion and should be fabricated and tested. In the case of spherical inclusions, our theory can be applied without further development. For a more extensive study that includes non-spherical shapes, we should try a hybrid method in which our analytical method for disordered MM uses the accurately evaluated permittivity and permeability-ordered MM by HFSS. There are several applications for thin-film rotators that can withstand high intensities.

(c) *Small antenna and magnetic mirror.* Although we focused on the near-IR region of the EM spectrum in the current program, our calculations are valid for the entire spectrum. In particular, the size reduction to antenna will be more useful in the RF regime where the current sizes are quite large. In addition, the MM magnetic mirror surface will be equally useful in achieving a low-profile antenna in that region of the spectrum. Design, fabrication, and demonstration of this concept at RF should be undertaken.

(d) *Counter-directed energy weapon.* The all-dielectric, thin-film, low-weight perfect reflector demonstrated in this program has an immediate advantage over existing technology for high-intensity resistant coating of DoD assets. We have approached the C-DEW program, and our request to synthesize and test large, self-assembled MM coatings is under consideration for funding.

REFERENCES

1 B. Slovick, Z.G. Yu and S. Krishnamurthy., *Phys. Rev. B.* **89**, 155118, 2014.

2 B. Slovick, Z.G. Yu, and S. Krishnamurthy., *Phys. Rev. B* **88**, 165116, 2013.

3 P. Moitra, B. Slovick, Z.G. Yu, S. Krishnamurthy, and J. Valentine, *Appl. Phys. Lett.* **104**, 171102 (2014); this work was highlighted in *Nature Photonics* **8**, 498, 2014.

4 P. Moitra, B. Slovick, W. Li, I. Kravchenko, D. Briggs, S. Krishnamurthy, and J. Valentine, *ACS Photonics*, (Accepted; May 15, 2015).

5 Z.G. Yu, B. Slovick, and S. Krishnamurthy, (manuscript in preparation for *Phys. Rev. Lett.*, 2015.).

6 Z.G. Yu, B. Slovick, and S. Krishnamurthy (manuscript in preparation for *Phys. Rev. **B***, 2015)

7 B. Slovick, P. Moitra, Z.G. Yu, S. Krishnamurthy, and J. Valentine (in preparation for *Nature Photonics*, 2015).

8 L. Lewin, J. IEEE (London) Part III 94, 65 (1947).

9 Y. Wu, J. Li, Z.-Q. Zhang, and C. T. Chan, *Phys. Rev. B* **74**, 085111-1, 2006.

10 O'Brien, S. and J. B. Pendry, *J. Phys.: Condens. Matter.* **14**, 4035-4044, 2002.

11 Kuester et al., *Prog. in EM Res. B* **33**, 175, 2011.

12 G. A. Niklasson, C. G. Granqvist, and O. Hunderi, *Appl. Optics* **20**, 26, 1981.

13 C. F. Bohren and D. R. Huffman, *Absorption and Scattering of Light by Small Particles* (Wiley 1998).

14 L. V. Wang and H. Wu, *Biomedical Optics: Principles and Imaging* (Wiley-Interscience 2007).

15 P. Sheng, *Scattering and Localization of Classical Waves in Random Media* (World Scientific 1990).

16 N. A. Khizhniak, *Sov. Phys. Tech. Phys.* **2**, 1858; 1865; 1877, (1957).

17 Y. Yang, W. Wang, P. Moitra, I. Kravchenko, D. P. Briggs, J. Valentine, *Nano Lett.* **14**, 1394, 2014.